Journal of Materials Chemistry A

PAPER

View Article Online
View Journal | View Issue

Cite this: J. Mater. Chem. A, 2017, 5, 12369

Unraveling factors leading to efficient norbornadiene–quadricyclane molecular solar-thermal energy storage systems†

Kjell Jorner,[ab] Ambra Dreos,[c] Rikard Emanuelsson,[ad] Ouissam El Bakouri,[e] Ignacio Fdez. Galván,[bf] Karl Börjesson,[cg] Ferran Feixas,*[e] Roland Lindh,*[bf] Burkhard Zietz,*[b] Kasper Moth-Poulsen*[c] and Henrik Ottosson*[ab]

Received 16th May 2017
Accepted 22nd May 2017

DOI: 10.1039/c7ta04259k

rsc.li/materials-a

Developing norbornadiene–quadricyclane (NBD–QC) systems for molecular solar-thermal (MOST) energy storage is often a process of trial and error. By studying a series of norbornadienes (**NBD-R$_2$**) doubly substituted at the C7-position with R = H, Me, and iPr, we untangle the interrelated factors affecting MOST performance through a combination of experiment and theory. Increasing the steric bulk along the **NBD-R$_2$** series gave higher quantum yields, slightly red-shifted absorptions, and longer thermal lifetimes of the energy-rich QC isomer. However, these advantages are counterbalanced by lower energy storage capacities, and overall R = Me appears most promising for short-term MOST applications. Computationally we find that it is the destabilization of the NBD isomer over the QC isomer with increasing steric bulk that is responsible for most of the observed trends and we can also predict the relative quantum yields by characterizing the S_1/S_0 conical intersections. The significantly increased thermal half-life of **NBD-iPr$_2$** is caused by a higher activation entropy, highlighting a novel strategy to improve thermal half-lives of MOST compounds and other photo-switchable molecules without affecting their electronic properties. The potential of the **NBD-R$_2$** compounds in devices is also explored, demonstrating a solar energy storage efficiency of up to 0.2%. Finally, we show how the insights gained in this study can be used to identify strategies to improve already existing NBD–QC systems.

Introduction

Widespread implementation of solar energy technologies is essential for the future development of a sustainable energy supply (or conversion) based entirely on renewable energy sources. Due to daily and yearly variations in both solar influx and energy demand, technologies for solar energy storage are particularly relevant.[1] Solar energy can be converted directly into latent chemical energy *via* several methods such as natural or artificial photosynthesis,[2,3] or photo-induced isomerization in chemical compounds – so-called molecular solar thermal (MOST) systems.[4] Since the initial idea to use photoinduced isomerizations for solar energy storage was conceived more than a century ago,[5] several molecular systems have been presented, including anthracene dimerization,[5,6] azobenzenes,[7] ruthenium fulvalene,[8,9] dihydroazulene–vinylheptafulvene[10] and norbornadiene–quadricyclane (NBD–QC).[11–18] From an applications perspective, many design challenges need to be addressed for the system to function efficiently.[13,19–21] Notably, a large fraction of the solar spectrum should be absorbed, the photoconversion must proceed with near unity quantum efficiency and the energy should be stored at a high energy density. Moreover, the photoisomer should be stable over time, the chemical compounds switchable for multiple cycles and the back-reaction from photoisomer to parent compound triggered externally by, *e.g.*, a solid state catalyst.

For the NBD–QC system (Fig. 1), several of these requirements are fulfilled, but unfortunately it only absorbs light below 300 nm.[13,21] NBD undergoes a photochemical [2 + 2]-cycloaddition reaction to form the strained high-energy QC isomer. Thermally, this reaction is forbidden according to the Woodward–Hoffmann rules[22] and the energy-releasing back-

[a]Department of Chemistry – BMC, Uppsala University, Box 576, SE-75123 Uppsala, Sweden. E-mail: henrik.ottosson@kemi.uu.se
[b]Department of Chemistry – Ångström Laboratory, Uppsala University, Box 523, SE-75120 Uppsala, Sweden
[c]Department of Chemistry and Chemical Engineering, Chalmers University of Technology, Kemigården 4, SE-41296 Gothenburg, Sweden
[d]Department of Engineering Sciences, Uppsala University, Box 534, SE-75121 Uppsala, Sweden
[e]Institut de Química Computacional i Catàlisi (IQCC), Departament de Química, Universitat de Girona, Campus Montilivi, 17003 Girona, Spain
[f]Uppsala Center of Computational Chemistry – UC$_3$, Uppsala University, Box 523, SE-75120 Uppsala, Sweden
[g]Department of Chemistry & Molecular Biology, University of Gothenburg, Kemigården 4, SE-41296 Gothenburg, Sweden

† Electronic supplementary information (ESI) available: Experimental procedures, spectral data for new compounds, computational details and Cartesian coordinates for calculated structures. See DOI: 10.1039/c7ta04259k

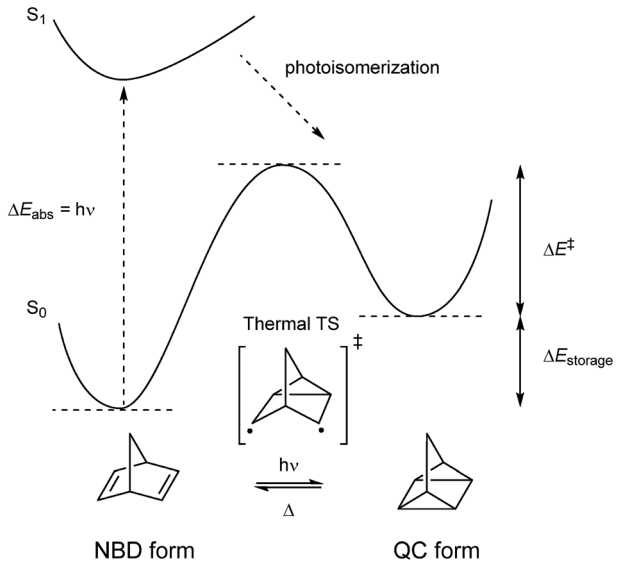

Fig. 1 Schematic figure of the thermal and photochemical isomerization between NBD and QC. Shown are the excitation energy, ΔE_{abs}, storage energy, $\Delta E_{storage}$, and activation energy for thermal back-reaction, $\Delta E^{\ddagger}$.

reaction from QC to NBD proceeds *via* a high-energy transition state (TS) of diradical character (experimental gas-phase activation energy of 33.5 kcal mol^{-1}).[18,23,24]

However, a challenge with the system is that all reported photoisomers of compounds with red-shifted absorption into the visible part of the spectrum have too short lifetimes to be practically useful for long-term energy storage applications,[4,12,14,20,25] and the quantum yields are often well below unity.[15] It is therefore desirable to develop a detailed understanding of how the NBD–QC system can be chemically engineered with respect to absorption spectrum, quantum yield, energy storage and barrier for the thermal back-reaction. Herein we report how to disentangle and balance the different factors influencing the efficiency of the NBD–QC system. We do this by a case study of three **NBD-R_2** molecules which carry the R = H, Me and iPr substituents on the C7 atom, giving different degrees of steric pressure on the NBD isomer (Fig. 2).

We observe that increased steric bulk leads to higher quantum yield for formation and an increased lifetime of the QC isomer, although these gains are balanced by a decrease in energy storage capacity. Importantly, we can rationalize the increase in quantum yields computationally by characterization

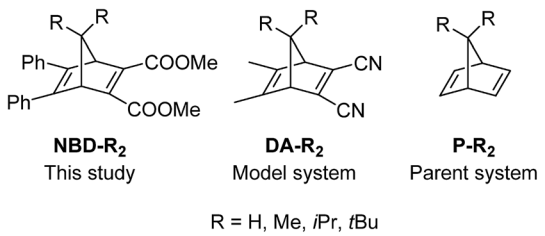

Fig. 2 NBD–QC systems investigated in this study. DA-R_2, P-R_2 and NBD-*t*Bu_2 are studied only computationally.

of the conical intersections through which the photochemical reaction occurs. One of us has previously shown that design and screening of NBDs with respect to spectral and energy storage characteristics can be performed computationally.[26] Now, for the first time also relative quantum yields can be predicted computationally. Furthermore, a simple DFT scheme is used to compute accurate enthalpy barriers for the thermal back-reactions. We expect that the insight and tools of this study will become important in the search for improved NBD/QC systems for MOST applications. At the end, the **NBD-R_2** molecules are evaluated in a solar energy conversion demonstration device, highlighting the possibility for future applications. The present results will also be important for NBD–QC systems considered as photo-switches, *e.g.*, in molecular electronics[27] and conjugated materials.[28]

Results and discussion

We reasoned that increasing the steric bulk going from R = H to Me and finally iPr would push the double bonds increasingly closer to each other, thereby increasing their interaction in a controlled way. Our initial hypothesis was that this mainly electronic effect would have a gradual influence on the properties of importance for MOST performance such as absorption spectrum and quantum yield. However, as we show below, this is only true for the absorption characteristics, and in fact the relative energies of the NBD and QC isomers, as affected by the steric pressure, is much more important.

In this section we first present the experimental characterization of the **NBD-R_2** series and then go on to untangle the reasons for the experimental trends by both experimental and computational investigations. After showing the use of **NBD-iPr_2** in a model MOST device, we finally demonstrate how the insights and computational methodology developed in this study can be used to identify strategies for improving known NBD compounds.

Synthesis and characterization

We synthesized **NBD-H_2**, **NBD-Me_2** and **NBD-iPr_2** and characterized their photophysical and photochemical properties (for experimental details, see the ESI†). **NBD-Me_2** has previously been reported.[12] We also considered synthesizing **NBD-*t*Bu_2** but discarded it for two reasons: (1) the **QC-*t*Bu_2** isomer is calculated to be more stable than **NBD-*t*Bu_2**, making it uninteresting for MOST applications, and, (2) the synthesis is considerably more challenging (see the ESI† for further discussion). However, we also include computational data for **NBD-*t*Bu_2** for comparison. The absorption spectra show peaks at 240 nm, 260 nm and 340 nm (Fig. 3) which are slightly red-shifted by 3–5 nm through substitution in the order **NBD-H_2** < **NBD-Me_2** < **NBD-iPr_2**, showing the effect of increased through-space interaction of the double bonds enforced by the steric bulk in line with our initial hypothesis. This observation is consistent with the calculated TD-DFT peaks (LC-τHCTH/6-311+G(2d,p), Table 1).[29–31]

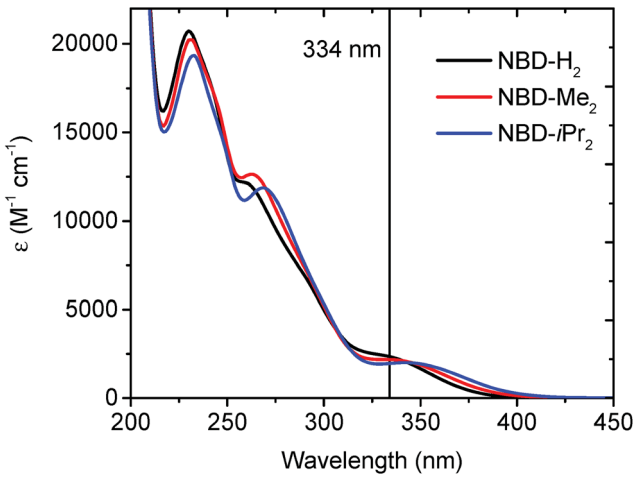

Fig. 3 Absorption spectra of NBD-H_2, NBD-Me_2 and NBD-iPr_2 in acetonitrile. Vertical bar shows wavelength for irradiation for the quantum yield measurements (334 nm, FWHM 2 nm).

Quantum yields for the NBD → QC isomerization after excitation with monochromatic light of 334 nm (FWHM 2 nm, Fig. 3) show an increase in the order **NBD-H$_2$** (0.73 ± 0.03) < **NBD-Me$_2$** (0.86 ± 0.10) < **NBD-iPr$_2$** (0.88 ± 0.04), although the difference between **NBD-Me$_2$** and **NBD-iPr$_2$** is not statistically significant (Table 1). The presence of isosbestic points testifies to clean photoreactions (Fig. S7–S9†). At the same time, the energy storage enthalpies as measured by differential scanning calorimetry (DSC) also decrease: 20.4 kcal mol^{-1} for **NBD-H$_2$**, 16.3 kcal mol^{-1} for **NBD-Me$_2$** and 11.1 kcal mol^{-1} for **NBD-iPr$_2$**, in fair agreement with the calculated DFT values (CAM-B3LYP-D3(BJ)/6-311+G(d,p)//PBE-D3(BJ)/6-31+G(d,p), Table 1).[32–35] There is also an increase in thermal half-lives of the QC isomers at 25 °C: 6.3 hours for **NBD-H$_2$**, 7.7 hours for **NBD-Me$_2$** and 56 hours for **NBD-iPr$_2$**. Although the experimental activation enthalpies ($\Delta H^{\ddagger}$) are approximately constant, in accordance with our calculations, a higher activation entropy ($\Delta S^{\ddagger}$) is affecting the half-life of **QC-iPr$_2$**, which is significantly longer than the other two (Tables 1 and S1,† *vide infra*). As the back-reaction from the QC to NBD for structurally very similar NBDs has been shown to be biradical in nature,[18] we do not expect any significant influence of the solvent on the kinetic parameters. In support of this the calculated activation enthalpies are invariant within 0.2 kcal mol^{-1} between the gas-phase, toluene and acetonitrile, consistent with a biradical mechanism (Table S8†).

Substantial effort has been made to tune thermal half-lives of the photo-stable isomers in MOST systems such as azoheteroarenes[36] and dihydroazulene–vinylheptafulvene.[37] This has been done also for NBD–QC by, *e.g.*, methyl substitution at bridgehead positions or placing trifluoromethyl groups on the bridges.[18,38] Based on the current results, we conclude that C7-substitution is a novel type of approach to achieve this kind of tuning in the NBD–QC system. Unfortunately, the beneficial increase in quantum yield and thermal lifetime with steric bulk is accompanied by a loss in the energy storage capacity. If shorter storage times are needed, **NBD-Me$_2$** can be considered the best candidate for MOST applications, otherwise the longer lifetime of the **NBD-iPr$_2$** system is needed.

Origin of the long half-life of QC-iPr$_2$

Why is the half-life of **QC-iPr$_2$** so long? We decided to investigate this further, aiming to find new ways of improving the NBD/QC system for MOST applications. The experimental $\Delta H^{\ddagger}$ values over the **QC-R$_2$** series are similar with 21.4 kcal mol^{-1} for **QC-H$_2$**, 21.5 kcal mol^{-1} for **QC-Me$_2$** and 21.7 kcal mol^{-1} for **QC-iPr$_2$**. The striking difference lies in $\Delta S^{\ddagger}$, which is approximately constant going from **QC-H$_2$** (−31.1 e.u.) to **QC-Me$_2$** (−32.2 e.u.), while that for **QC-iPr$_2$** is much more negative (−45.3 e.u.). At room temperature, this contributes a difference of ca 1 kcal mol^{-1} in $\Delta G^{\ddagger}$. It turns out that the underlying reason is due to increased steric crowding in the NBD isomer that hinders the rotation of the iPr groups while they are free to rotate in the QC isomer. As the TS lies between the two isomers, it will experience some of the hindered rotation and this results in the more negative $\Delta S^{\ddagger}$ for R = iPr.

Indeed, in support of our hypothesis the ^{1}H NMR signals of **NBD-iPr$_2$** at room temperature are much broader than those of **QC-iPr$_2$**, indicating the presence of hindered rotation.[39] Therefore, we carried out variable temperature ^{1}H NMR experiments in $CDCl_3$ to confirm this. The spectra of a 50 : 50 mixture of NBD and QC isomers (Fig. 4a) clearly show several signals for the NBD isomer at −32 °C (slow rotation on NMR timescale) which

Table 1 Experimental and calculated properties of NBD-R_2 compounds

	ϕ^a	$\Delta H_{storage}{}^b$ (kcal mol^{-1})	$t_{1/2}{}^c$ (hours)	$\Delta H^{\ddagger c}$ (kcal mol^{-1})	$\lambda_{pos}{}^d$ (nm)	$A_{onset}{}^e$ (nm)
NBD-H$_2$	0.73 ± 0.03	20.4 (19.7)	6.3	21.4 (19.6)	341 (330)	391
NBD-Me$_2$	0.86 ± 0.10	16.3 (16.7)	7.7	21.5 (19.0)	346 (339)	403
NBD-iPr$_2$	0.88 ± 0.04	11.1 (13.9)	56	21.7 (19.8)	349 (343)	414
NBD-*t*Bu$_2$	—	—(−2.9)	—	—(30.6)	—(375)	—

[a] Quantum yield in acetonitrile after excitation at 334 nm. [b] Measured by differential scanning calorimetry (DSC). Calculated CAM-B3LYP-D3(BJ)/6-311+G(d,p)//PBE-D3(BJ)/6-31+G(d,p) energies in parenthesis. [c] Derived from Eyring plot in toluene. Calculated CAM-B3LYP-D3(BJ)/6-311+G(d,p)/SMD = toluene//PBE-D3(BJ)/6-31+G(d,p) values in parenthesis. [d] Absorption maximum, given for the lowest-energy absorption peak and obtained by spectral deconvolution using four Gaussian peaks. Calculated LC-τHCTH/6-311+G(2d,p)/SMD = acetonitrile//PBE-D3(BJ)/6-31+G(d,p) values in parenthesis. [e] Absorption onset defined as log(ε) = 2.

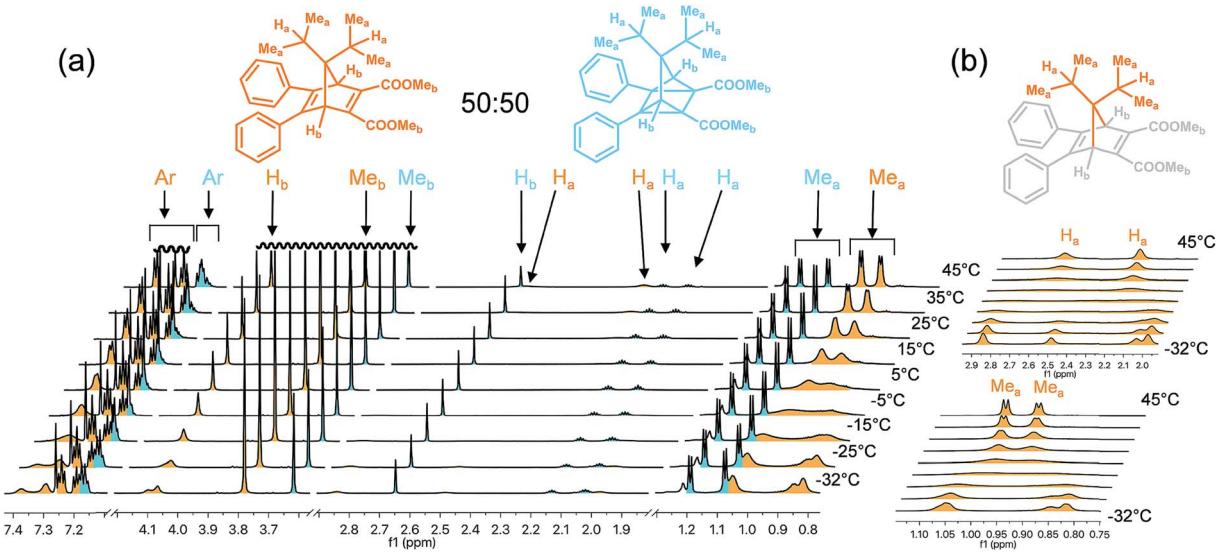

Fig. 4 (a) ^{1}H NMR spectra of a 50 : 50 mixture of NBD and QC isomers of **NBD-iPr$_2$** at temperatures from −32 °C to 45 °C in $CDCl_3$. Peaks originating from the NBD isomer are shown in orange and those from the QC isomer in blue. Axis has been broken to show the regions of interest. (b) ^{1}H NMR spectra at temperatures from −32 °C to 45 °C in $CDCl_3$ for methyl (red) and methine (orange) protons of a sample of pure NBD isomer of **NBD-iPr$_2$**. "Ar" means aryl protons, "Me" means methyl protons and "H" means tertiary protons as shown in the structures. For experimental details and full spectra, see the ESI, Section 3.†

are broadened with increasing temperature and have coalesced at 45 °C (fast rotation on NMR timescale). This is especially clear for the methyl and methine protons of the iPr groups as seen in the temperature-dependent ^{1}H NMR spectrum of pure **NBD-iPr$_2$** (Fig. 4b). The presence of several conformers at the lower temperature is further confirmed by chemical exchange peaks in the NOESY spectrum at −32 °C that disappear at 45 °C (Fig. S1 and S2†). Also, we see weak NOE peaks between the bridgehead and iPr methyl protons and the phenyl protons for NBD but not for QC supporting the increased steric congestion in the NBD isomer (Fig. S3–S6†). The hindered rotation in **NBD-iPr$_2$** described here is similar to that previously seen in 7,7-aryl-substituted norbornanes which have analogous temperature-dependent ^{1}H NMR spectra.[40] In contrast, the ^{1}H peaks of the QC isomer are not affected over this temperature range (Fig. 4a), indicating free rotation of the iPr groups. The room-temperature ^{1}H NMR spectra of **NBD-iPr$_2$** and **QC-iPr$_2$** display the same behavior in toluene-d_8 as in $CDCl_3$, showing that the hindered rotation is not sensitive to the solvent (Fig. S66†).

The increased activation entropy of **QC-iPr$_2$** → **NBD-iPr$_2$** as compared to R = H and Me points to a new strategy in the design of MOST materials with longer thermal half-lives, where the activation enthalpy and entropy can potentially be tuned independently of each other. This strategy seems particularly promising for extending the thermal stability of photoswitchable materials without making large changes to otherwise advantageous electronic properties.

Quantum chemical calculations

To decipher the factors responsible for the experimental trends we turned to quantum-chemical calculations. To evaluate the effect of steric bulk on the relative energies of the NBD and QC isomers, we calculated the reaction **NBD-R$_2$**/**QC-R$_2$** + 2H$_2$ → **NBD-H$_2$**/**QC-H$_2$** + 2R–H. The energy release, ΔE_{rel}, increases by 2.9 kcal mol^{-1} from **NBD-Me$_2$** (−32.9 kcal mol^{-1}) to **NBD-iPr$_2$** (−35.8 kcal mol^{-1}), while it is nearly constant from **QC-Me$_2$** (−29.6 kcal mol^{-1}) to **QC-iPr$_2$** (−29.9 kcal mol^{-1}), demonstrating that the decrease in energy storage capacity (calculated value of 2.6 kcal mol^{-1}) is almost entirely due to increased steric repulsion in the NBD isomer while the QC isomer is mostly unaffected. Consistent with this finding, the decrease in $\Delta H_{storage}$ can also be related to the Taft steric constant E_S, although the relation is non-linear (Fig. 5).[41]

To rationalize the trend in quantum yields we located the minimum energy conical intersections (CIs) between the S_1 and

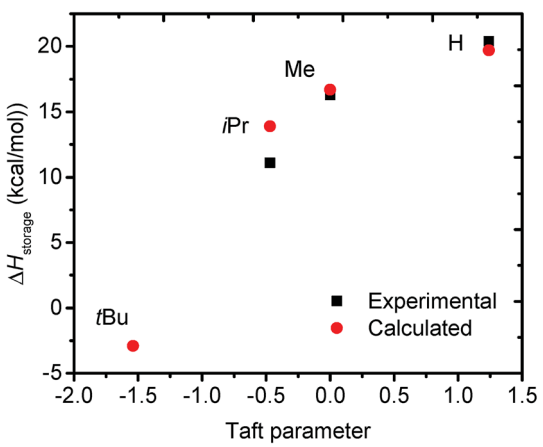

Fig. 5 Relation between the Taft steric parameter E_s and $\Delta H_{storage}$ for **NBD-R$_2$**. Experimental values are given in black and computed values in red.

S_0 states for **NBD-H_2** and **NBD-Me_2** using 2-state-average (2-SA-) CASSCF(2in2)/6-31G(d) calculations (see ESI, section 9 for full details†).[42–44] It is known that photoisomerization for **P-H_2** occurs efficiently after triplet sensitization with quantum yields of up to 0.91, and only *ca.* 0.05 for direct irradiation.[20] Donor–acceptor NBDs (DA-NBDs) with electron-donating and electron-accepting substituents show reverse reactivity with one study giving a quantum yield of 0.68 under direct irradiation and only 0.06–0.15 with triplet sensitization.[45] As the **NBD-R_2** compounds are also DA-NBDs, and as the photoreactions are performed under oxygen-containing atmosphere with high quantum yields, it is reasonable to assume that the present photoreactions also proceed through the singlet state. Furthermore, Goodson and co-workers recently reported that the photoconversion of a derivative of **NBD-H_2** with –COOEt instead of –COOMe substituents was not affected by the triplet quencher 1,3-cyclohexadiene.[18]

So what is the mechanism of the singlet state isomerization? A rhombically distorted S_1/S_0 CI for **P-H_2** was previously located by Antol using MR-CIS.[46] This CI preferentially leads back to the NBD isomer, in agreement with experiment. However, no similar studies of DA-NBDs have been reported yet. Yamazaki hypothesized that the switch from S_1 to T_1 photoreactivity from **P-H_2** to DA-NBDs is due to a larger ionic character in the S_1 state of the latter.[45] Indeed, we find that while the **P-H_2** exhibits a symmetrical, rhombically distorted CI structure with C–C distances of 1.948 Å (compared to 1.987 Å with MR-CIS),[46] that for **NBD-H_2** has one shorter bond which is almost fully formed (1.730 Å) while the other remains long (2.210 Å) (Fig. 6). The C–C lengths for **NBD-Me_2** are 1.737 Å and 2.196 Å, while **NBD-iPr_2** could not be calculated due to its large size. The NPA charges[47] of S_1 and S_0 in the vicinity of the CI geometries support Yamazaki's hypothesis of larger ionic character as **NBD-H_2** has a larger charge polarization than **P-H_2** with positive charge on the donor side and negative charge on the acceptor side (Fig. 6).[48] There are also shallow minima on the S_1 surface in between the Franck–Condon (FC) geometry and the CIs, but the depth (0.4 kcal mol^{-1} for **P-H_2** and 3.2 kcal mol^{-1} for **NBD-H_2** with 3-SA-CASSCF(2in2)) is small compared to the excess energy

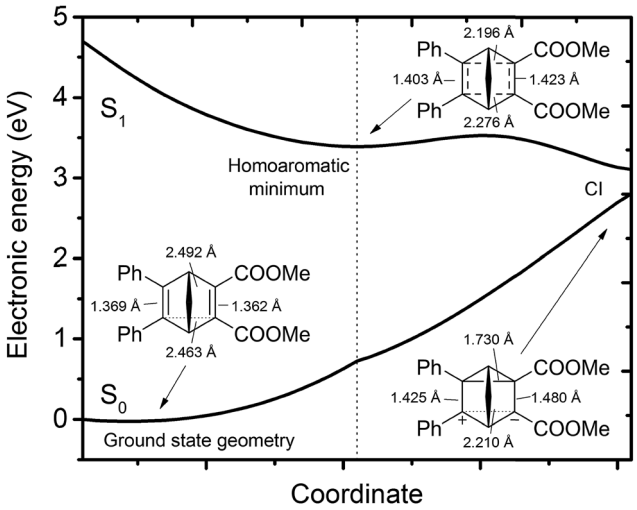

Fig. 7 S_0 and S_1 energies for **NBD-H_2** along the path from the optimized S_0 minimum to the optimized S_1 minimum to the CI at the 3-SA-CASSCF/6-31G(d) level. The points between the optimized structures have been obtained by linear interpolation in internal coordinates.

from the FC point (29.0 kcal mol^{-1} for **P-H_2** and 30.1 kcal mol^{-1} for **NBD-H_2** at the same level) and they are not likely to be populated significantly (for further discussion, including the effect of dynamical correlation, see the ESI†). An overview of the PES for **NBD-H_2** is given in Fig. 7.

Characterization of the CIs reveals a dramatic difference in terms of relaxation pathways (Fig. 8a and b).[49] The CI for **P-H_2** has one dominant relaxation direction towards the NBD isomer, which is consistent with the very low quantum yield for direct irradiation. On the contrary, the CIs for **NBD-H_2** and **NBD-Me_2** have plausible relaxation pathways to both the NBD and QC isomers. For **P-R_2** the difference in gradient of relaxation to NBD and QC ($\Delta Gradient_{CI}$) decreases with increasing steric bulk, but remains large even with R = *t*Bu and the effect on the quantum yield should be small. For **NBD-R_2** on the other hand the relaxation pathways are almost equally viable. Consequently, going from **NBD-H_2** to **NBD-Me_2** should favor relaxation to the

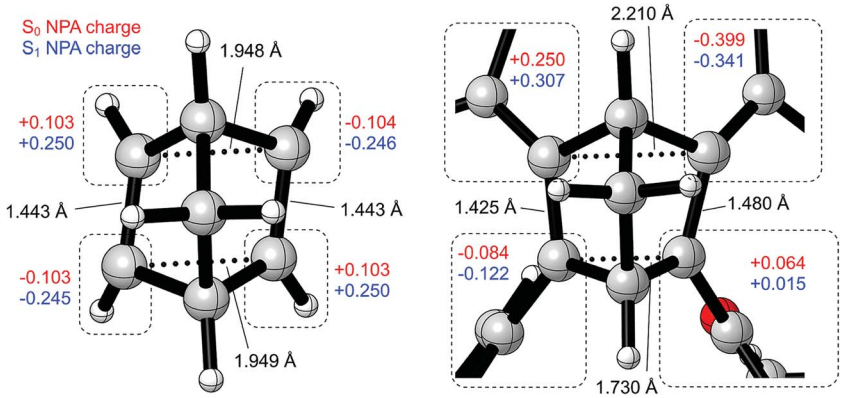

Fig. 6 Conical intersection geometries for P-H_2 (left) and NBD-H_2 (right) at the 2-SA-CASSCF(2in2)/6-31G(d) level. NPA charges in the vicinity of the CIs are given as a sum for the carbon atom in question and its substituents (the distinction between the S_0 and S_1 states is not possible at the exact CI position).

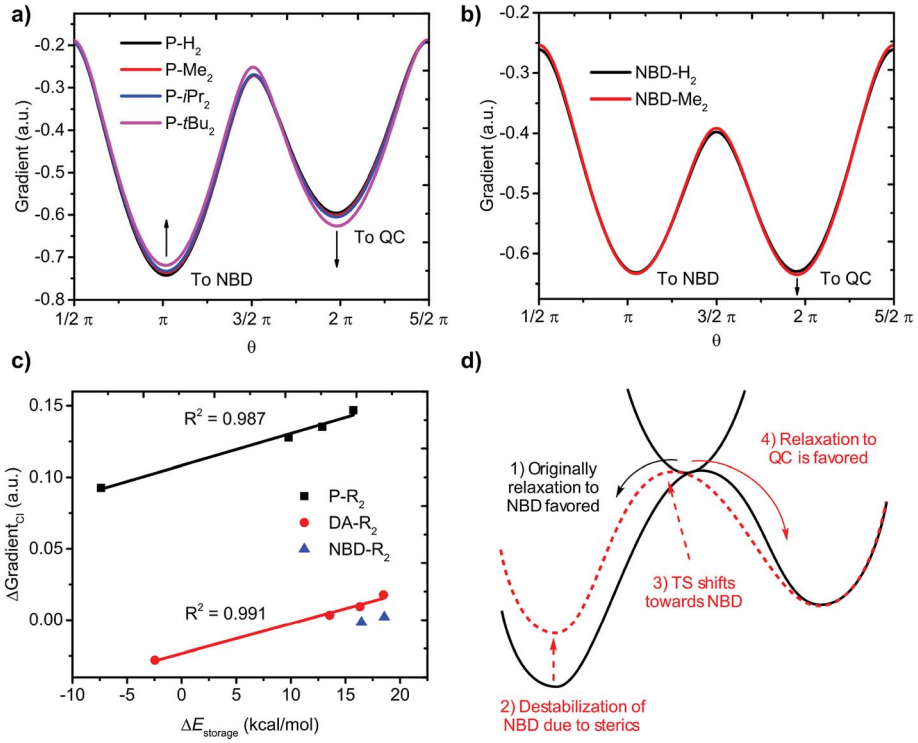

Fig. 8 (a) CI analysis for **P-R$_2$** (b) CI analysis for **NBD-H$_2$** and **NBD-Me$_2$**. (c) Correlation between energy difference between NBD and QC isomers and gradient difference between the relaxation pathways to NBD and QC. (d) Effect of NBD destabilization on TS position and relaxation pathways from the CI. θ is the angular coordinate in the branching plane that lifts the degeneracy of the CI.

QC isomer, consistent with the observed increase in quantum yield. These trends are also seen for **DA-R$_2$** with the full range of R = H, Me, iPr and *t*Bu (Fig. S20†).

Interestingly, there is an almost perfect linear correlation between $\Delta E_{storage}$ and $\Delta Gradient_{CI}$ for both the **P-R$_2$** and **DA-R$_2$** systems with R^2 values of 0.987 and 0.991, respectively (Fig. 8c), meaning that a lower energy storage capacity is associated with a higher quantum yield for both systems. For **NBD-R$_2$** there are only two points but they also follow this trend. We rationalize this finding by applying the Hammond postulate.[50] By decreasing the energy difference between the NBD and QC isomers, the TS is moved towards the NBD side of the reaction coordinate (Fig. 8d). If the excited state potential energy surface is not affected to an equal extent, the CI empties on the S_0 surface closer to the QC side with decreasing energy difference, which leads to a more efficient photoreaction. This explanation is corroborated by excellent correlations between calculated extent of bond formation in the S_0 TS and $\Delta E_{storage}$ for both **P-R$_2$**, **DA-R$_2$** and **NBD-R$_2$** (Fig. S40†). It is therefore not the increased electronic interaction between the double bonds due to steric bulk but rather the decreased energy difference between the NBD and QC isomers which is responsible for the increase in quantum yield.

Although dynamics should be considered to get a rigorous understanding of how the quantum yields are affected by substitution, the present calculations show that steric bulk at the C7 position can perturb the potential energy surfaces around the CI in a manner consistent with more favorable relaxation to the QC isomer. It is likely that other ways of changing the relative energy of the NBD and QC isomers, besides substitution at C7, will have similar effects on the quantum yields that can now be predicted with the computational model given above. It would also be illuminating to explore the effects of dynamical correlation on the CI characterization, but this was not feasible at present.

Nature of the S_1 state minimum

As the shallow S_1 minimum (Fig. 7) could potentially affect the quantum yield negatively if it gets too deep, we decided to investigate its nature further to see how it can be avoided. Based on our previous interest in excited state aromaticity[51] we hypothesized that the minimum could be stabilized by homoaromaticity[52] in the S_1 state with four electrons in the cycle (aromatic according to Baird's rule for the excited state).[51] To this end, we calculated the multicenter indices (MCIs) of the CASSCF wave functions at the S_1 minima of **P-H$_2$**, **DA-H$_2$** and **NBD-H$_2$**.[53] The resulting values (0.032, 0.024 and 0.021) are large and approach that of the S_2 state cyclobutadiene at its D_{2h} ground state geometry (0.049) which was previously assessed as clearly aromatic.[54] The homoaromaticity is also corroborated by qualitative S_1 NICS scans which show the characteristic minima of aromatic compounds (see the ESI†).[55,56] While the MCI values decrease from **P-H$_2$** to **DA-H$_2$** and **NBD-H$_2$**, the depth of the minima at the same time increases along with the increasing donor–acceptor character (0.4 kcal mol^{-1} for **P-H$_2$**, 2.1 kcal mol^{-1} for **DA-H$_2$** and 3.2 kcal mol^{-1} for **NBD-H$_2$** at the CASSCF

level). Therefore, the less S_1-homoaromatic compounds have the deeper minima. Fortunately, the depth of the minimum is decreased going from **NBD-H$_2$** (3.2 kcal mol^{-1}) to **NBD-Me$_2$** (2.3 kcal mol^{-1}), so steric pressure is effective in suppressing this potentially detrimental minimum. Nevertheless, it appears that stronger donor–acceptor character of the NBD than that seen here could be detrimental to the MOST performance as it leads to a deeper minimum from where decay would lead to the NBD isomer which would reduce the quantum yield.

MOST application

After having untangled the different factors affecting the properties along the **NBD-R$_2$** series, we went on to evaluate their performance for MOST applications. For this purpose, we chose **NBD-iPr$_2$** as it shows a useful half-life of 56 hours, enabling day-to-day storage. We used a custom-made microfluidic device[17,57] with an irradiated area of 4 cm^2 and a channel depth of 60 μm (Fig. 9). A 50 mM solution of **NBD-iPr$_2$** in toluene was circulated through the flow cell, and the conversion of **NBD-iPr$_2$** to **QC-iPr$_2$** was monitored by ^{1}H NMR spectroscopy. The back-conversion of **QC-iPr$_2$** to **NBD-iPr$_2$** releases 16.3 kcal mol^{-1}, according to DSC (*vide supra*). The solar energy storage rate at the working conditions of the device is 2.4 Js^{-1} m^{-2}, with a solar energy storage efficiency η_{MOST} = 0.2% (see the ESI, Section 8, for details†). This efficiency could be increased in different ways, for example by increasing the solubility (higher concentration), increasing the path length of the collector, or decreasing the residence time (as shown in ref. 9). Design of NBD systems with more red-shifted onset of absorption should lead to higher energy storage efficiencies,[17] while the solar harvesting efficiency observed here is two orders of magnitude higher than a previous ruthenium fulvalene based MOST system, due to a much higher quantum yield of the NBD/QC system.[9,57] Hence, it is comparable to the 0.1% and 1.1% achieved recently by some of us with a different pair of NBDs.[17] Although we use a flow device here, it has been shown previously that NBDs can be incorporated in solid polymers films which show photoswitching with negligible degradation after 1000 cycles.[12] There is therefore potential to construct solid-state MOST devices with NBDs that could be used when solvent is impractical.

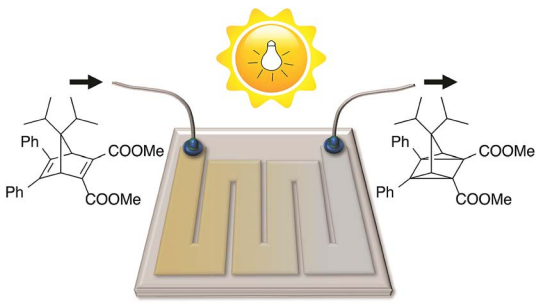

Fig. 9 Schematic representation of the microfluidic device used to test the performance of NBD-iPr$_2$ for MOST applications. A solution of NBD-iPr$_2$ in toluene-d$_8$ was circulated through the device at a constant flow rate, while irradiated with a lamp simulating the solar spectrum.

Experimental predictions based on the presented methodology

Can the insights gained from the **NBD-R$_2$** series be used to design new or improved NBDs for MOST applications? In a recent series of studies one of us designed and synthesized **MQ-H$_2$** (Table 2) and showed its potency in a hybrid device combining solar heating and molecular thermal storage.[15,17] Using the device described above it displayed η_{MOST} = 1.1%, clearly superior to the 0.2% of **NBD-iPr$_2$**. Could increasing the steric bulk from **MQ-H$_2$** to **MQ-Me$_2$** improve this performance even further, *e.g.*, by improving the low quantum yield of 0.28? Our calculated storage enthalpies and activation enthalpies for **MQ-H$_2$** are in good agreement with experiment, while the peak absorption calculated by TD-DFT is too high by *ca.* 0.2 eV (also seen in the original article[17]). Upon Me-substitution, the calculated energy storage enthalpy is lowered from 24.8 to 21.7 kcal mol^{-1} (ca 13%) while the activation enthalpy increases only slightly (21.4 *vs.* 21.9 kcal mol^{-1}). The excitation energy is lowered somewhat from 3.30 to 3.26 eV (374 *vs.* 380 nm). These trends are the same as seen for **NBD-R$_2$**. We located the CIs for the NBD → QC interconversion and find a steeper gradient for

Table 2 Experimental and calculated properties of MQ-R$_2$ compounds

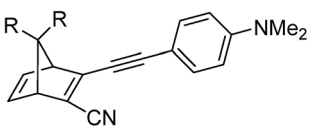

MQ-R$_2$ R = H, Me

	ϕ	$\Delta H_{storage}$ (kcal mol^{-1})	$t_{1/2}$ (hours)	$\Delta H^{\ddagger}$ (kcal mol^{-1})	λ_{pos} (nm)	A_{onset} (nm)
MQ-H$_2$ exp.	0.28	24.6	5.05	22.1	398	456
MQ-H$_2$ calc.	—	24.8	—	21.4	374	—
MQ-Me$_2$ calc.	—	21.7	—	21.9	380	—

relaxation to NBD than QC, in line with the quantum yield of only 0.28 (Fig. S44†). For **MQ-Me$_2$**, the gradient difference becomes smaller, indicating that the quantum yield should be increased as compared to **MQ-H$_2$**. We therefore predict that **MQ-Me$_2$** will show a higher quantum yield and a lower energy storage than **MQ-H$_2$**, and future experiments will be needed to reveal which one would overall be best for MOST applications.

Conclusions and outlook

In summary, we have shown that the quantum yields and thermal lifetimes of a series of DA-NBDs are increased with larger steric bulk at the C7 carbon. However, the energy storage capacity simultaneously decreases and on balance **NBD-Me$_2$** with a quantum yield of (0.86 ± 0.10), an energy storage capacity of 16.3 kcal mol^{-1} and a thermal half-life of 7.6 hours at 25 °C is the best alternative for short-term MOST applications. It was found that the significantly longer thermal half-life of 56 hours for **NBD-iPr$_2$** is mainly caused by a more negative activation entropy due to hindered rotation of the iPr groups in the TS. This points to a new strategy in the design of thermally stable MOST compounds and other photo-switchable molecules where the activation enthalpy and entropy could be tuned independently. The potential of the **NBD-R$_2$** compounds for MOST applications was demonstrated by incorporation of **NBD-iPr$_2$** in a microfluidic flow reactor with a solar energy storage efficiency $\eta_{MOST} = 0.2\%$, two orders of magnitude better than a previous ruthenium fulvalene system. We explain the increased thermal lifetime and decreased storage capacity of **NBD-Me$_2$** and **NBD-iPr$_2$** as compared to **NBD-H$_2$** due to higher steric repulsion in the NBD isomer than in the QC isomer. The increased quantum yields were rationalized by quantum-chemical characterizations of the S_0/S_1 conical intersections. We believe that the present study paves the way for rational design of new NBD-QC systems using computational tools, where quantum yields, energy storage capacities and thermal lifetimes can be finely balanced for optimal performance. Along these lines, we presented calculations showing how the low quantum yields of one of the currently most promising NBDs, **MQ-H$_2$**, should be improved by methyl substitution in **MQ-Me$_2$**.

Acknowledgements

Prof. Adolf Gogoll is acknowledged for fruitful discussions on the NMR investigations. H. O. acknowledges the Swedish Research Council (grants 2015-04538 and 2011-04177) for financial support. The Swedish NMR centre at the University of Gothenburg is acknowledged for support. K. M. P. and A. D. acknowledges the K. & A. Wallenberg foundation and the Swedish Foundation for Strategic Research for financial support. K. B. acknowledge the Swedish Foundation for Strategic Research and the Ragnar Söderberg foundation for financial support. O. E. B. and F. F. acknowledge the Ministerio de Economía y Competitividad of Spain (projects CTQ2014-54306-P and CTQ2014-59212-P) and the Generalitat de Catalunya (project 2014SGR931, Xarxa de Referència en Química Teòrica i Computacional, and grant No. 2014FI_B 00429 to O. E. B.). R. L. and I. F. G. acknowledge the Swedish Research Council (grants 2012-3910 and 2016-03398) for financial support. We also thank NSC, Linköping, within the Swedish National Infrastructure for Computing (SNIC), Sweden, for the allotment of computer time.

References

1 (*a*) N. S. Lewis and D. G. Nocera, *Proc. Natl. Acad. Sci. U. S. A.*, 2006, **103**, 15729–15735; (*b*) T. R. Cook, D. K. Dogutan, S. Y. Reece, Y. Surendranath, T. S. Teets and D. G. Nocera, *Chem. Rev.*, 2010, **110**, 6474–6502.

2 A. Magnuson, M. Anderlund, O. Johansson, P. Lindblad, R. Lomoth, T. Polivka, S. Ott, K. Stensjö, S. Styring, V. Sundström and L. Hammarström, *Acc. Chem. Res.*, 2009, **42**, 1899–1909.

3 S. Berardi, S. Drouet, L. Francas, C. Gimbert-Surinach, M. Guttentag, C. Richmond, T. Stoll and A. Llobet, *Chem. Soc. Rev.*, 2014, **43**, 7501–7519.

4 A. Lennartson, A. Roffey and K. Moth-Poulsen, *Tetrahedron Lett.*, 2015, **56**, 1457–1465.

5 F. Weigert, *Jahrbuch für Photographie, Kinematographie und Reproduktionsverfahren*, 1909, p. 109.

6 G. Jones II, T. E. Reinhardt and W. R. Bergmark, *Sol. Energy*, 1978, **20**, 241–248.

7 (*a*) T. J. Kucharski, N. Ferralis, A. M. Kolpak, J. O. Zheng, D. G. Nocera and J. C. Grossman, *Nat. Chem.*, 2014, **6**, 441–447; (*b*) A. M. Kolpak and J. C. Grossman, *Nano Lett.*, 2011, **11**, 3156–3162; (*c*) K. Ishiba, M. Morikawa, C. Chikara, T. Yamada, K. Iwase, M. Kawakita and N. Kimizuka, *Angew. Chem., Int. Ed.*, 2015, **54**, 1532–1536; (*d*) W. Luo, Y. Feng, C. Cao, M. Li, E. Liu, S. Li, C. Qin, W. Hu and W. Feng, *J. Mater. Chem. A*, 2015, **3**, 11787–11795; (*e*) A. K. Saydjari, P. Weis and S. Wu, *Adv. Energy Mater.*, 2016, **7**, 1601622.

8 (*a*) K. P. C. Vollhardt and T. W. Weidman, *J. Am. Chem. Soc.*, 1983, **105**, 1676–1677; (*b*) R. Boese, J. K. Cammack, A. J. Matzger, K. Pflug, W. B. Tolman, K. P. C. Vollhardt and T. W. Weidman, *J. Am. Chem. Soc.*, 1997, **119**, 6757–6773; (*c*) K. Börjesson, D. Ćoso, V. Gray, J. C. Grossman, J. Guan, C. B. Harris, N. Hertkorn, Z. Hou, Y. Kanai, D. Lee, J. P. Lomont, A. Majumdar, S. K. Meier, K. Moth-Poulsen, R. L. Myrabo, S. C. Nguyen, R. A. Segalman, V. Srinivasan, W. B. Tolman, N. Vinokurov, K. P. C. Vollhardt and T. W. Weidman, *Chem.–Eur. J.*, 2014, **20**, 15587–15604.

9 K. Moth-Poulsen, D. Ćoso, K. Börjesson, N. Vinokurov, S. K. Meier, A. Majumdar, K. P. C. Vollhardt and R. A. Segalman, *Energy Environ. Sci.*, 2012, **5**, 8534–8537.

10 A. B. Skov, S. L. Broman, A. S. Gertsen, J. Elm, M. Jevric, M. Cacciarini, A. Kadziola, K. V. Mikkelsen and M. B. Nielsen, *Chem.–Eur. J.*, 2016, **22**, 14567–14575.

11 C. Philippopoulos, D. Economou, C. Economou and J. Marangozis, *Ind. Eng. Chem. Prod. Res. Dev.*, 1983, **22**, 627–633.

12 S. Miki, Y. Asako and Z. Yoshida, *Chem. Lett.*, 1987, **16**, 195–198.

13 Z. Yoshida, *J. Photochem.*, 1985, **29**, 27–40.

14 V. Gray, A. Lennartson, P. Ratanalert, K. Börjesson and K. Moth-Poulsen, *Chem. Commun.*, 2014, **50**, 5330–5332.
15 M. Quant, A. Lennartson, A. Dreos, M. Kuisma, P. Erhart, K. Börjesson and K. Moth-Poulsen, *Chem.–Eur. J.*, 2016, **22**, 13265–13274.
16 U. Bauer, S. Mohr, T. Döpper, P. Bachmann, F. Späth, F. Düll, M. Schwarz, O. Brummel, L. Fromm, U. Pinkert, A. Görling, A. Hirsch, J. Bachmann, H.-P. Steinrück, J. Libuda and C. Papp, *Chem.–Eur. J.*, 2017, **23**, 1613–1622.
17 A. Dreos, K. Börjesson, Z. Wang, A. Roffey, Z. Norwood, D. Kushnir and K. Moth-Poulsen, *Energy Environ. Sci.*, 2016, **22**, 627–633.
18 K. J. Spivack, J. V. Walker, M. J. Sanford, B. R. Rupert, A. R. Ehle, J. M. Tocyloski, A. N. Jahn, L. M. Shaak, O. Obianyo, K. M. Usher and F. E. Goodson, *J. Org. Chem.*, 2017, **82**, 1301–1315.
19 K. Börjesson, A. Lennartson and K. Moth-Poulsen, *ACS Sustainable Chem. Eng.*, 2013, **1**, 585–590.
20 A. D. Dubonosov, V. A. Bren and V. A. Chernoivanov, *Russ. Chem. Rev.*, 2002, **71**, 917–927.
21 T. J. Kucharski, Y. Tian, S. Akbulatov and R. Boulatov, *Energy Environ. Sci.*, 2011, **4**, 4449–4472.
22 R. B. Woodward and R. Hoffmann, *The Conservation of Orbital Symmetry*, Verlag Chemie, Weinheim, 1970.
23 H. M. Frey, *J. Chem. Soc.*, 1964, 365–367.
24 C. Qin, Z. Zhao and S. R. Davis, *J. Mol. Struct.: THEOCHEM*, 2005, **728**, 67–70.
25 (*a*) Y. Harel, A. W. Adamson, C. Kutal, P. A. Grutsch and K. Yasufuku, *J. Phys. Chem.*, 1987, **91**, 901–904; (*b*) W. L. Dilling, *Chem. Rev.*, 1966, **66**, 373–393.
26 (*a*) M. J. Kuisma, A. M. Lundin, K. Moth-Poulsen, P. Hyldgaard and P. Erhart, *J. Phys. Chem. C*, 2016, **120**, 3635–3645; (*b*) M. Kuisma, A. Lundin, K. Moth-Poulsen, P. Hyldgaard and P. Erhart, *ChemSusChem*, 2016, **9**, 1786–1794.
27 (*a*) E. E. Bonfantini and D. L. Officer, *J. Chem. Soc., Chem. Commun.*, 1994, 1445; (*b*) P. Lainé, V. Marvaud, A. Gourdon, J.-P. Launay, R. Argazzi and C.-A. Bignozzi, *Inorg. Chem.*, 1996, **35**, 711–714; (*c*) S. Fraysse, C. Coudret and J.-P. Launay, *Eur. J. Inorg. Chem.*, 2000, **2000**, 1581–1590; (*d*) H. Löfås, B. O. Jahn, J. Wärnå, R. Emanuelsson, R. Ahuja, A. Grigoriev, H. Ottosson, P. Ordejon, J. M. Pruneda, D. Sanchez-Portal and J. M. Soler, *Faraday Discuss.*, 2014, **76**, 105–124; (*e*) B. E. Tebikachew, H. B. Li, A. Pirrotta, K. Börjesson, G. C. Solomon, J. Hihath and K. Moth-Poulsen, *J. Phys. Chem. C*, 2017, **121**, 7094–7100.
28 (*a*) M. Maafi, C. Lion and J. J. Aaron, *Synth. Met.*, 1996, **83**, 167–169; (*b*) F. Babudri, G. Bilancia, A. Cardone, P. Coppo, L. De Cola, G. M. Farinola, J. W. Hofstraat and F. Naso, *Photochem. Photobiol. Sci.*, 2007, **6**, 361–364.
29 (*a*) A. D. Boese and N. C. Handy, *J. Chem. Phys.*, 2002, **116**, 9559–9569; (*b*) H. Iikura, T. Tsuneda, T. Yanai and K. Hirao, *J. Chem. Phys.*, 2001, **115**, 3540–3544.
30 R. Krishnan, J. S. Binkley, R. Seeger and J. A. Pople, *J. Chem. Phys.*, 1980, **72**, 650–654.
31 M. J. Frisch, *et al.*, *Gaussian 09 (Revision E.01)*, Gaussian, Inc., Wallingford CT, 2009, The complete reference can be found in the ESI.
32 T. Yanai, D. P. Tew and N. C. Handy, *Chem. Phys. Lett.*, 2004, **393**, 51–57.
33 J. P. Perdew, K. Burke and M. Ernzerhof, *Phys. Rev. Lett.*, 1996, **77**, 3865–3868.
34 S. Grimme, S. Ehrlich and L. Goerigk, *J. Comput. Chem.*, 2011, **32**, 1456–1465.
35 A. V. Marenich, C. J. Cramer and D. G. Truhlar, *J. Phys. Chem. B*, 2009, **113**, 6378–6396.
36 J. Calbo, C. E. Weston, A. White, H. Rzepa, J. Contreras-García and M. J. Fuchter, *J. Am. Chem. Soc.*, 2016, **139**, 1261–1274.
37 (*a*) M. Cacciarini, A. B. Skov, M. Jevric, A. S. Hansen, J. Elm, H. G. Kjaergaard, K. V. Mikkelsen and M. Brøndsted Nielsen, *Chem.–Eur. J.*, 2015, **21**, 7454–7461; (*b*) M. Cacciarini, M. Jevric, J. Elm, A. U. Petersen, K. V. Mikkelsen and M. B. Nielsen, *RSC Adv.*, 2016, **6**, 49003–49010; (*c*) M. H. Hansen, J. Elm, S. T. Olsen, A. N. Gejl, F. E. Storm, B. N. Frandsen, A. B. Skov, M. B. Nielsen, H. G. Kjaergaard and K. V. Mikkelsen, *J. Phys. Chem. A*, 2016, **120**, 9782–9793.
38 (*a*) T. Nagai, K. Fujii, I. Takahashi and M. Shimada, *Bull. Chem. Soc. Jpn.*, 2001, **74**, 1673–1678; (*b*) T. Nagai, I. Takahashi and T. Nishikubo, *Chem. Lett.*, 2003, **32**, 754–755.
39 D. Casarini, L. Lunazzi and A. Mazzanti, *Eur. J. Org. Chem.*, 2010, **2010**, 2035–2056.
40 D. Casarini, S. Grilli, L. Lunazzi and A. Mazzanti, *J. Org. Chem.*, 2004, **69**, 345–351.
41 R. W. Taft, *J. Am. Chem. Soc.*, 1952, **74**, 2729–2732.
42 B. O. Roos, P. R. Taylor and P. E. M. Siegbahn, *Chem. Phys.*, 1980, **48**, 157–173.
43 F. Aquilante, J. Autschbach, R. K. Carlson, L. F. Chibotaru, M. G. Delcey, L. De Vico, I. Fdez. Galván, N. Ferré, L. M. Frutos, L. Gagliardi, M. Garavelli, A. Giussani, C. E. Hoyer, G. Li Manni, H. Lischka, D. Ma, P. Å. Malmqvist, T. Müller, A. Nenov, M. Olivucci, T. B. Pedersen, D. Peng, F. Plasser, B. Pritchard, M. Reiher, I. Rivalta, I. Schapiro, J. Segarra-Martí, M. Stenrup, D. G. Truhlar, L. Ungur, A. Valentini, S. Vancoillie, V. Veryazov, V. P. Vysotskiy, O. Weingart, F. Zapata and R. Lindh, *J. Comput. Chem.*, 2016, **37**, 506–541.
44 R. Ditchfield, W. J. Hehre and J. A. Pople, *J. Chem. Phys.*, 1971, **54**, 724–728.
45 H. Ikezawa, C. Kutal, K. Yasufuku and H. Yamazaki, *J. Am. Chem. Soc.*, 1986, **108**, 1589–1594.
46 I. Antol, *J. Comput. Chem.*, 2013, **34**, 1439–1445.
47 (*a*) A. E. Reed, R. B. Weinstock and F. Weinhold, *J. Chem. Phys.*, 1985, **83**, 735–746; (*b*) E. D. Glendening, J. K. Badenhoop, A. E. Reed, J. E. Carpenter, J. A. Bohmann, C. M. Morales, C. R. Landis and F. Weinhold, *NBO 6.0*, Theoretical Chemistry Institute, University of Wisconsin, Madison, 2013.
48 C. Y. Legault, *CYLview 1.0b*, Université de Sherbrooke, 2009, http://www.cylview.org.
49 I. Fdez. Galván, M. G. Delcey, T. B. Pedersen, F. Aquilante and R. Lindh, *J. Chem. Theory Comput.*, 2016, **12**, 3636–3653.
50 G. S. Hammond, *J. Am. Chem. Soc.*, 1955, **77**, 334–338.

51 (*a*) N. C. Baird, *J. Am. Chem. Soc.*, 1972, **94**, 4941–4948; (*b*) H. Ottosson, *Nat. Chem.*, 2012, **4**, 969–971; (*c*) M. Rosenberg, C. Dahlstrand, K. Kilså and H. Ottosson, *Chem. Rev.*, 2014, **114**, 5379–5425; (*d*) R. Papadakis and H. Ottosson, *Chem. Soc. Rev.*, 2015, **44**, 6472–6493.
52 R. V. Williams, *Chem. Rev.*, 2001, **101**, 1185–1204.
53 (*a*) P. Bultinck, R. Ponec and S. Van Damme, *J. Phys. Org. Chem.*, 2005, **18**, 706–718; (*b*) E. Matito, *ESI-3D: electron sharing indexes program for 3D molecular space partitioning*, Institute of Computational Chemistry and Catalysis, Girona, 2006, http://www.iqc.udg.es/~eduard/ESI.
54 F. Feixas, J. Vandenbussche, P. Bultinck, E. Matito and M. Solà, *Phys. Chem. Chem. Phys.*, 2011, **13**, 20690–20703.
55 (*a*) A. Stanger, *J. Org. Chem.*, 2006, **71**, 883–893; (*b*) J. O. C. Jiménez-Halla, E. Matito, J. Robles and M. Solà, *J. Organomet. Chem.*, 2006, **691**, 4359–4366.
56 K. Aidas, *et al.*, *Wiley Interdiscip. Rev.: Comput. Mol. Sci.*, 2014, **4**, 269–284. The complete reference can be found in the ESI.†
57 K. Börjesson, D. Dzebo, B. Albinsson and K. Moth-Poulsen, *J. Mater. Chem. A*, 2013, **1**, 8521–8524.